J Appl Physiol 129: 483–491, 2020.
First published July 9, 2020; doi:10.1152/japplphysiol.00133.2020.

RESEARCH ARTICLE

Mapping the relationships between joint stiffness, modeled muscle stiffness, and shear wave velocity

Andrew D. Vigotsky,[1] Elliott J. Rouse,[2] and Sabrina S. M. Lee[3]

[1]*Departments of Biomedical Engineering and Statistics, Northwestern University, Evanston, Illinois;* [2]*Neurobionics Lab, Department of Mechanical Engineering, University of Michigan, Ann Arbor, Michigan; and* [3]*Department of Physical Therapy and Human Movement Sciences, Northwestern University, Chicago, Illinois*

Submitted 25 February 2020; accepted in final form 30 June 2020

Vigotsky AD, Rouse EJ, Lee SSM. Mapping the relationships between joint stiffness, modeled muscle stiffness, and shear wave velocity. *J Appl Physiol* 129: 483–491, 2020. First published July 9, 2020; doi:10.1152/japplphysiol.00133.2020.—Joint stiffness is often measured to make inferences about the stiffness of muscle groups, but little can be gleaned about individual muscles. Decomposing the muscular origins of joint stiffness may inform treatment targets for conditions like spasticity. To complement joint stiffness, shear wave ultrasound elastography has been used to estimate the material properties of individual muscles. If shear wave measures are to be used to assess the muscular origins of joint stiffness, then changes in shear wave velocity should strongly relate to changes in joint stiffness. Here, we estimated the relationships between shear wave velocity in the primary plantar flexors [soleus (SOL) and medial gastrocnemius (MG)] and ankle joint stiffness. Participants performed isometric plantar flexion tasks at a range of activations (0–40%), while joint stiffness and muscle shear wave velocities were obtained. We observed a strong, linear relationship between plantar flexor shear wave velocities and joint stiffness. Remarkably, the parameter estimates of this stiffness-shear wave relationship strongly agreed with theoretical and literature-based estimates [SOL:MG parameter ratios = 2.83 (observed) vs. 2.85 (expected from theoretical stiffness ratio)]. Finally, a musculoskeletal model of the plantar flexors was able to accurately reproduce joint stiffness estimates, and shear wave velocities could explain 80–95% of the variance in modeled muscle stiffness. These findings suggest that shear wave velocity may be used to infer the muscular origins of changes in joint stiffness.

NEW & NOTEWORTHY Shear wave velocity is commonly assessed to infer the muscular origins of changes in joint stiffness, but the exact relationship between shear wave velocity changes in muscle and joint stiffness changes remains unknown. Here, we systematically evaluated and quantified this relationship in the plantar flexors. Our results provide evidence for the ability of shear wave velocity to elucidate the muscular origins of joint stiffness changes.

INTRODUCTION

Joint stiffness dynamically refines the mechanical interface between a human and the surrounding world. From an external perspective, joint stiffness determines how joints respond to a positional perturbation. From an internal perspective, joint stiffness determines how easily a joint can be maneuvered by the muscles that span it. Although ligaments and joint capsules contribute to joint stiffness, under active conditions, it is primarily determined by muscles surrounding the joint (36). Thus, joint stiffness is often assessed to infer its muscular origins (4, 50, 53, 56). A clearer picture of the etiology of joint stiffness may help with diagnosis and treatment of musculoskeletal disorders, as well as expand our fundamental understanding of human movement (36).

There are two primary approaches used to measure joint stiffness, but neither provide insight into its anatomical underpinnings. The first, more popular approach, estimates quasi-stiffness (not true stiffness in dynamic conditions) by differentiating the net joint moment-angle relationship (37, 51). Quasi-stiffness assumes stationarity and negligible higher-order impedance terms, such as damping and inertia. Moreover, quasi-stiffness cannot be assessed when the system is static, as there is no change in joint angle. The second approach uses system identification analyses to separate stiffness from higher-order contributors to joint impedance, such as inertia and damping (36, 52, 54). In addition, because system identification approaches rely on small perturbations, stiffness can also be obtained during quasi-static tasks. When assessing joint stiffness, the joint is modeled as a black box mechanical system, and little information is gleaned about the properties of the tissues that surround the joint. Greater anatomical resolution would allow for an improved understanding of joint stiffness, as recent work suggests that muscle-dependent changes in joint stiffness are muscle-specific (35).

Neuromusculoskeletal models allow for the study of the mechanics of the musculoskeletal system and its concomitant neural control, including the origins of joint stiffness (13). One current but limited approach for estimating muscle stiffness is through the use of such models (1, 32). When modeling muscle stiffness, musculotendon units (MTUs) are represented as springs that act upon a joint as determined by their moment arm (1, 32). While these models may predict emergent, system-level stiffness, such as end-point stiffness (32), they rely on computation and several model-specific assumptions. Reliance on computations may limit their clinical applicability, while assumptions introduce uncertainties that may—especially in populations with pathology—be violated. Therefore, empirical approaches to assess muscle mechanical properties are warranted.

Ultrasound shear wave (SW) elastography can be used to assess muscle material properties, such as mechanical properties under passive and active conditions. Changes in SW velocity occur depending on muscle length and the level of activation (14). This method has been used to investigate changes in mechanical properties in muscles with pathology

Correspondence: A. D. Vigotsky (vigotsky@u.northwestern.edu).

(38, 39), following training and stretching interventions (2, 3, 34), and to answer basic muscle mechanics questions, such as determining muscle slack length (31). Recent work has also demonstrated that SW propagation depends on both the mechanical properties of a tissue and stresses within the tissue (10, 33, 42). However, the relationship between SW velocity and joint stiffness remains elusive (9, 22, 25, 35, 38, 39). These questions are complementary to those answered by assessing joint stiffness, in that SW elastography assesses individual muscles, while joint stiffness represents the net effect of all tissues that act on a joint. Thus, the difference in anatomical specificity between joint stiffness and SW velocity makes their relationship ambiguous. Alternatively, while models of muscle stiffness provide similar anatomical resolution to SW elastography, they are distinct constructs. Therefore, it remains unclear how SW velocity relates to joint-level assessments and modeled muscle stiffness (15–17).

Relationships between joint- and muscle-level assessments of stiffness need to be evaluated to deepen our scientific and clinical understanding of these measurements. In particular, if clinicians or researchers are to use SW ultrasound to gain insight into the muscle-specific etiology of changes in joint stiffness, then SW velocity changes should parallel changes in joint stiffness. Furthermore, modeled muscle stiffness can be related to empirical SW measures for an improved understanding of SW on the muscle- rather than joint-level (32). The purpose of this work was to quantify the relationships between joint stiffness, modeled muscle stiffness, and SW velocity to provide insight into muscle-dependent changes in joint stiffness. In line with biomechanical theory, we expected that plantar flexor SW velocity would be strongly and positively associated with joint stiffness and that the recorded SW velocities would positively correlate with modeled muscle stiffness. Such a finding would lend credence to the use of SW for understanding the muscular origins of joint stiffness changes.

METHODS

Participants

Ten healthy, young adults (6 females, 4 males; age = 26 ± 4 yr; body mass = 69 ± 16 kg; height = 1.7 ± 0.1 m) participated in this study. Each participant was free from lower extremity musculoskeletal or neuromuscular pathology or pain for at least 1 yr before participation, and provided informed consent before beginning. This study was approved by the Northwestern University Institutional Review Board (IRB no. STU00202024). Parts of this work have been presented previously (57, 58).

Experimental Setup

Data were collected from each participant over two sessions, which were separated by at least 48 h; one day was dedicated to a knee-flexed position, while the other was dedicated to a knee-extended position. Each participant sat in a customized dynamometer, the Neurobionics Rotary Dynamometer—a custom frame-mounted motor (BSM90N-3150AF; Baldor, Fort Smith, AR) with a six-axis load cell (45E15A4, JR3, Woodland, CA) coupled to an adjustable chair (835-000, Biodex Medical Systems, Shirley, NY) (6)—with their hips flexed to 85° and the ipsilateral (right) ankle positioned at 90° (foot relative to shank). The sagittal plane ankle axis of rotation (lateral malleolus) was placed collinearly with that of the motor using a laser pointer. The knee was positioned to 0° (extended) or 90° (flexed) (Fig. 1). Surface electromyography electrodes were placed over the muscle bellies of the medial gastrocnemius (MG), lateral gastrocnemius (LG), soleus (SOL), and tibialis anterior (TA), in positions that would not interfere with ultrasound transducer placement. Although electromyographical data were collected, those data were not analyzed and will not be presented here.

Ultrasonography

Ultrasound images were obtained from the MG muscle-tendon junction (MTJ) (B-mode only) and the muscle bellies of the MG, SOL, and TA (B-mode and SW) (Aixplorer SuperSonic Imagine, Aix-en-Provence, France). Ultrasound field of view was 49 mm, and the depth and gain were manually adjusted for each muscle to maximize its visibility. For both Achilles tendon stiffness and moment

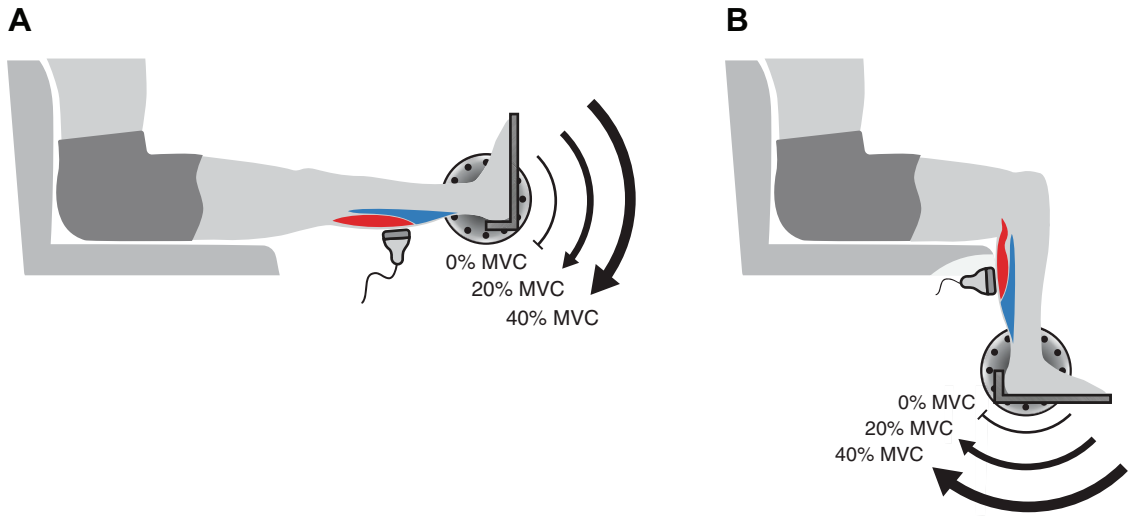

Fig. 1. Experimental setup. Participants performed isometric plantar flexion trials at 0, 20, and 40% of maximum voluntary contraction with the knee fully extended (*A*) and with the knee flexed at 90° (*B*). Shear wave velocities in the medial gastrocnemius (red), soleus (blue), and tibialis anterior (not shown) were obtained with shear wave ultrasound elastography. Note that, since the medial gastrocnemius is a biarticular muscle, it was placed in active insufficiency when the knee was flexed (*B*). MVC, maximum voluntary contraction.

arm estimates, three video trials (26 Hz) of the MG MTJ were captured on the distal posteromedial aspect of the MG, while the transducer was held using a neoprene strap. Shear wave (1 Hz) and B-mode (10 Hz) images were obtained from the midbellies of the MG and TA, and the SOL was imaged through the midbelly of the LG. Data from the MG and SOL were collected so that they could be decoupled via active insufficiency of the MG in the knee flexed condition (Fig. 1), and the TA was collected as a negative control, as its activation during an isometric plantar flexion task is negligible (49). Notably, we did not measure the LG SW velocity due to time constraints and its presumed collinearity with the MG.

To enable fast transitions between the perturbation and imaging trials, the transducer was loosely secured to the next muscle belly to be imaged using a custom neoprene strap. The strap was tight enough to hold the transducer in position between trials and allow for some movement when manually handled, but not so tight that it hindered natural changes in muscle shape during contraction. The neoprene strap was connected to a custom molded transducer holder, which was designed to ensure the transducer would not press directly on the skin; liberal quantities of gel were used to ensure images could be obtained while allowing for bulging. During SW imaging trials, the transducer was manually handled to obtain images in the fascicle plane; careful attention was given to minimize pressure on the muscle. Shear wave images were obtained using the musculoskeletal foot and ankle presets (optimization, persistence, and smoothing parameters of std, none, and none, respectively), capable of measuring a maximum SW velocity of 14.1 m/s. A 1 cm $\times$ 1 cm region of interest was used to obtain estimates of SW group velocities; if needed, this region was then cropped to exclude anatomical structures other than the muscle belly of interest (e.g., aponeuroses, other muscles), which was only necessary in a few images/participants and resulted in minimal loss of the region of interest ($\leq$0.3 cm^2 decrease). The company software provides a proprietary "quality factor" value to indicate the "quality" of each SW velocity measurement for each pixel. This is related to the cross-correlation algorithm that the company software uses to track the propagation of SWs through the tissue (38). Because blank pixels would have a quality factor lower than 0.8, they were excluded by default; all collected images were included in our analyses. Shear wave velocities within the cropped region of interest with a quality factor of $\geq$0.8 were averaged for each trial (35, 38, 39).

Protocol

Plantar and dorsiflexion maximum voluntary contractions (MVC) were first collected over three, 5-s trials for each direction. Net plantar flexion moments from the MVC trials were low-pass filtered with a fifth-order, zero-lag Butterworth filter with a 6-Hz cutoff frequency. The peak value from each trial was obtained, and the average of the peak values from the three MVC trials was used for subsequent trials and analyses. Live visual feedback of normalized plantar flexion net joint moments was provided during each trial, along with the target MVC. The participant was asked to maintain their net joint moment at the target MVC for the duration of the trial. Subjective experimenter discretion was used in the event that a participant did not properly complete the task (namely, stopping before the trial was complete, not matching the target MVC before the trial began, or if notable drift was present), and the trial was discarded and repeated; we note that such trials were rare. Because of the randomization employed, it is unlikely that this substantially biased the results (i.e., due to learning or fatigue).

Two sets of trials were used to collect data for our primary outcomes: *1*) those with perturbations, which were used to obtain estimates of joint stiffness and *2*) those without perturbations, which were used to obtain SW velocities. In both sets of trials, participants performed isometric plantar flexion tasks at 0, 20, and 40% MVC, so as to create considerable spread in joint stiffnesses and SW velocities, while limiting the fatigue and SW saturation that would emerge with higher levels of activation (Fig. 1). During perturbation trials, sagittal plane, filtered Gaussian white noise perturbations with a mean amplitude of 1° and a cutoff frequency of 5 Hz were applied to each participant's ankle. To approximate the muscle state during static SW trials (36), small amplitudes and low frequencies were chosen to better represent short-range stiffness and limit reflex contributions, respectively. During SW trials, the same setup was used, but no perturbations were applied. All kinetic (three-dimensional forces and moments) and kinematic (sagittal plane ankle angle) data were sampled at 2,500 Hz.

Shear wave images were recorded from the SOL, MG, and TA muscles in a randomized fashion. Each muscle was randomized to be imaged during the first third, middle third, or last third of the experiment, and the order of activations was randomized within each muscle. A total of six SW images were taken for each activation for each muscle. Ten-second perturbation trials were collected in a randomized order between SW trials, for a total of 27 trials per activation. Twenty-seven trials was chosen to keep the 95% confidence interval (CI) of the stiffness estimates for a given activation to be less than $\pm$10% of the mean stiffness estimate for that activation. For example, the randomized protocol would take a form similar to $MG20_{1-3}$, perturbations 1–9, $MG20_{4-6}$, $MG0_{1-3}$, perturbations 10–18, . . ., etc., until all 81 perturbation trials and 27 SW trials were completed. In the event that a participant became uncomfortable (e.g., paresthesia in their foot), the foot was released from the plastic orthotic until the participant felt ready to resume. Shear wave trials were then binned according to their condition (0, 20, or 40% MVC).

For inputs to the musculotendon model, Achilles tendon characteristics were estimated by imaging the MG MTJ. Specifically, Achilles tendon stiffness was estimated from MG MTJ displacements during ramp isometric plantar flexion contractions (0–60% MVC) at a rate of $36/\pi$% MVC/s over three separate trials. A trial was repeated when the transducer lost contact with the skin due to muscle bulging or when the MTJ moved outside of the field of view.

Joint Stiffness

Raw data collected during the perturbation trials were analyzed using a system identification method described previously (41). Briefly, using all trials for a given activation, an impedance impulse-response function (IRF) was estimated from the pseudoinverse of the autocorrelation matrix and an averaged time-varying and time-invariant cross-correlation. The time-varying portion of the algorithm was used to account for any changes in strategy, which was evidenced by nonzero moments out of plane. The impedance IRFs were numerically integrated to obtain joint stiffness estimates. Each participant's 27 trials were analyzed together, such that the system identification algorithm would produce one estimate. Reflex stiffness analyses based on the IRF were also run to ensure reflex contributions were minimal.

Musculoskeletal Models of Joint and Muscle Stiffness

We developed two musculoskeletal models to better understand musculotendon contributors to joint stiffness, and to relate the modeled muscle stiffness estimates to measured SW velocities. Our first model, developed a priori, was a simple, lumped muscle model, in which the triceps surae was modeled as two springs in series, consisting of a muscle spring and a tendon spring. However, because the lumped muscle model produced implausible estimates of muscle stiffness, we developed another model post hoc. The second model—a discrete muscle model—incorporates all three muscles of the triceps surae and was scaled in accordance with literature values. Herein, we describe the models in greater detail.

Lumped Muscle Model (a priori). A biomechanical model was created in MATLAB (2018a, MathWorks, Natick, MA) to estimate muscle stiffness (k^M). First, moment arms (r) for the passive trials were estimated using MG moment arms from OpenSim (Stanford, CA) (5, 21); the moment arms were not scaled since the effect of

scaling was assumed to be negligible. To account for increases in moment arm during activation due to bulging, moment arm values for active trials were multiplied by 1.185 (29); it was assumed that the difference between the 20 and 40% MVC conditions was negligible, as the change in moment arm between low levels of activation appears miniscule (23). Second, using each participant's moment arm estimate, tendon force $\left(F^T = \frac{M_{net}}{r}\right)$ was calculated from ramp contraction trials. Tendon elongation was calculated from the experimental data (MTJ tracked B-mode ultrasound images, Tracker, Douglas Brown, https://www.physlets.org) (61). Tendon forces and the associated tendon elongations (i.e., MTJ displacement) were then used to estimate tendon stiffness $\left(k^T = \frac{dF^T}{dL^T}\right)$. Finally, the muscle was modeled to be in series with the tendon, which acts about the joint center from a distance, its moment arm. Thus, a net joint moment can be defined as

$$M_{net} = \frac{k^T k^M}{k^T + k^M}\left(\Delta L^{MT}\right)(r),$$

where ΔL^{MT} is the MTUs theoretical excursion from "resting length". Mechanically, the derivative of M_{net} with respect to the joint angle is joint stiffness,

$$\frac{dM_{net}}{d\theta} = \frac{k^T k^M}{k^T + k^M}\left[\frac{dr}{d\theta}\Delta L^{MT} + r^2\right],$$

from which k^M could be estimated.

Discrete Muscle Model (post hoc). Because the simple biomechanical model yielded implausible results (see RESULTS), a more complex model was created post hoc in MATLAB. This model was based on previous work by Hu et al. (32), who modeled upper extremity end-point stiffness using discrete MTUs. All three muscles of the triceps surae (MG, SOL, and LG) were incorporated, which were parameterized by scaling literature values and muscle stiffness (19, 32). Muscle activations—or relative muscle forces (62)—were calculated by minimizing the sum of squared activations, while satisfying task constraints (net joint moment and position) (18, 32, 45); no electromyography data were used for this optimization. Muscle activations, architecture, and geometry were used to estimate both muscle and joint stiffnesses. To address the post hoc nature of the model, its parameter degrees of freedom, and the potential for "overfitting", the model was developed and parameterized using simulated data; only after obtaining reasonable joint stiffness outputs was the model run and verified with experimental data. Details of model construction and parameterization can be found in the APPENDIX and Table S1 (see www.doi.org/10.17605/osf.io/d49pb; all Supplemental Materials may be found at this website).

Statistical Analysis

To assess the linear relationships between *1*) joint moment, knee position, and SW velocity; *2*) joint stiffness and SW velocity; and *3*) modeled muscle stiffness and SW velocity, statistical analyses were carried out in R (version 3.5.2) (8, 48). First, we used hierarchical linear models (HLM) to independently regress SOL, MG, and TA SW velocities on ankle net joint moment condition, knee position, and the position-by-moment interaction. The position-by-moment interaction indicated the extent to which the two knee positions uncoupled the measurements obtained from each muscle. Second, an HLM was used to assess the relationship between joint stiffness (response variable) and both SOL and MG SW velocities (independent regressors), where SW velocities were averaged within condition, since there existed no natural pairing for the repeated trials. A repeated-measures correlation was used to directly assess the extent to which these independent regressors—SOL and MG SW velocities—were orthogonalized by our inclusion of two knee positions (7, 12). Third, HLMs were used to assess the association between modeled muscle stiffness from the discrete muscle model and SW velocity of the MG or SOL. For all HLMs, data were nested within participants, and varied slopes and intercepts were permitted. Model fits were assessed using root mean square error (RMSE) and coefficients of determination (R^2), which were calculated using the variance (σ^2) of the model residuals before (unconditional, σ_u^2) and after (conditional, σ_c^2) adding the variable(s) of interest: $R^2 = 1 - \sigma_c^2/\sigma_u^2$ (59).

To verify the discrete muscle model with experimental data, Lin's concordance correlation coefficients (40) (CCC) were calculated to quantify the absolute agreement between empirical and modeled joint stiffnesses.

Finally, we assessed the intrasession repeatability of our SW velocity measures using all six SW trials for each condition. A single full factorial linear mixed-effects model (8) was used to estimate an adjusted intraclass correlation coefficient (aICC) (44), which considered both of the primary muscles investigated (MG and SOL), the two knee position conditions, and all activation levels. Repeatability of these measures is necessary to meet the assumptions of our primary analysis, in that there should be negligible error for our independent variable, SW velocity.

For all RMSEs, coefficients of determination, and CCCs, 95% confidence intervals (CI) were estimated using a nonparametric bootstrap, in which the data were resampled with replacement on the participant level for a total of 1,000 replicates. An estimation rather than null-hypothesis significance testing approach was taken to avoid the dichotomization of evidence (20, 24). Thus, no a priori α-level was defined; rather, evidence was interpreted continuously using a combination of statistical outcomes, plausibility of effects, and data quality (43). Data are presented as an estimate (95% CI), unless otherwise indicated.

RESULTS

Shear wave velocities in the MG and SOL had an aICC of 0.791 after adjusting for muscle, activation, and knee position, indicating our intrasession SW velocities were fairly repeatable. Representative ultrasound images can be seen in Supplemental Fig. S1.

Shear Wave Velocity Versus Net Joint Moment

To evaluate how well the experimental paradigm uncoupled the SOL and MG, we constructed HLMs to evaluate the effects of position and moment on muscle SW velocity. Hierarchical linear models accurately represented the relationships between SOL SW velocity and net joint moments [$R^2 = 0.87$ (0.83, 0.93); RMSE = 0.66 m/s (0.54, 0.80)] and MG SW velocity and net joint moments [$R^2 = 0.89$ (0.85, 0.95); RMSE = 0.53 m/s (0.37, 0.66)] (Fig. 2, *A* and *B*; Supplemental Table S2). However, HLMs failed to capture much of the variance in TA SW velocity [$R^2 = 0.38$ (0.18, 0.52); RMSE = 0.33 m/s (0.24, 0.43)] (Fig. 2*C*; Supplemental Table S2).

Joint Stiffness Versus Shear Wave Velocity

A multivariable HLM, consisting of MG and SOL SW velocities as regressors and joint stiffness as the response variable, was able to capture nearly all of the variance in joint stiffness [$R^2 = 0.96$ (0.94, 0.97); RMSE = 15 N·m/rad (13, 20)] (Fig. 3, Table 1). Repeated-measures correlations indicated that our experimental protocol was successful in drastically attenuating the collinearity between MG and SOL SW velocities, from $r = 0.93$ (0.87, 0.97) with just knee extension

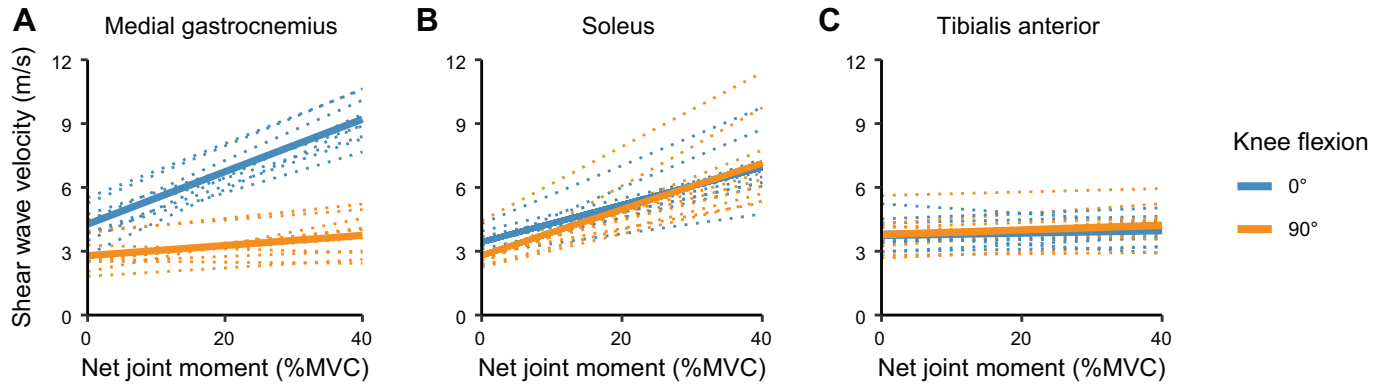

Fig. 2. Relationships between shear wave velocity and ankle net joint moment. *A*: medial gastrocnemius shear wave velocity has a knee condition-dependent relationship with net plantar flexor joint moment. *B*: soleus shear wave velocity has a knee condition-independent relationship with net plantar flexor joint moment. *C*: tibialis anterior shear wave velocity is not related to net plantar flexor joint moment or knee condition. Solid lines indicate constant estimates (i.e., pooled or fixed effects), and dotted lines indicate varying effects (i.e., individual or random effects). MVC, maximum voluntary contraction.

to $r = 0.46$ (0.28, 0.66) with both knee flexion and extension. Importantly, the high R^2s and low RMSEs observed are suggestive that the muscle state was similar during perturbation and SW trials.

Modeled Muscle Stiffness (Lumped Model)

Modeled muscle stiffness estimates were evaluated and deemed implausible. Specifically, participants' median ± interquartile range stiffnesses were 134 ± 238 N/mm, with a range of 14–78,604 N/mm. No further analyses were performed using these data.

Verification of Modeled Joint Stiffness (Discrete Muscle Model)

Measures of absolute agreement (CCC and RMSE) were used to verify the discrete muscle model. For both the flexed [CCC = 0.97 (0.96, 0.98); RMSE = 12 N·m/rad (9, 15)] and extended [CCC = 0.85 (0.81, 0.89); RMSE = 38 N·m/rad (27, 48)] knee conditions, the discrete muscle model performed well in predicting joint stiffness (Fig. 4).

Modeled Muscle Stiffness (Discrete Muscle Model) Versus Shear Wave Velocity

Modeled muscle stiffness estimates of the MG and SOL were regressed on MG and SOL SW velocities, respectively. In the MG, SW velocity explained 80% of the variance in modeled muscle stiffness [$R^2 = 0.80$ (0.71, 0.86); RMSE = 37 N/mm (34, 45)], and in the SOL, SW velocity explained 95% of the variance in modeled muscle stiffness [$R^2 = 0.95$ (0.91, 0.95); RMSE = 24 N/mm (23, 32)] (Fig. 5).

DISCUSSION

Joint Stiffness and Shear Wave Velocity

Our findings elucidate the relationship between SW velocity in the MG and SOL muscles and ankle joint stiffness. We decoupled the biarticular plantar flexors (gastrocnemii) from the primary uniarticular plantar flexor (SOL) by including both knee flexion and extension conditions (Fig. 2, *A* and *B*). In contrast to previous work, which assessed quasi-stiffness between individuals in passive conditions (15–17), we used

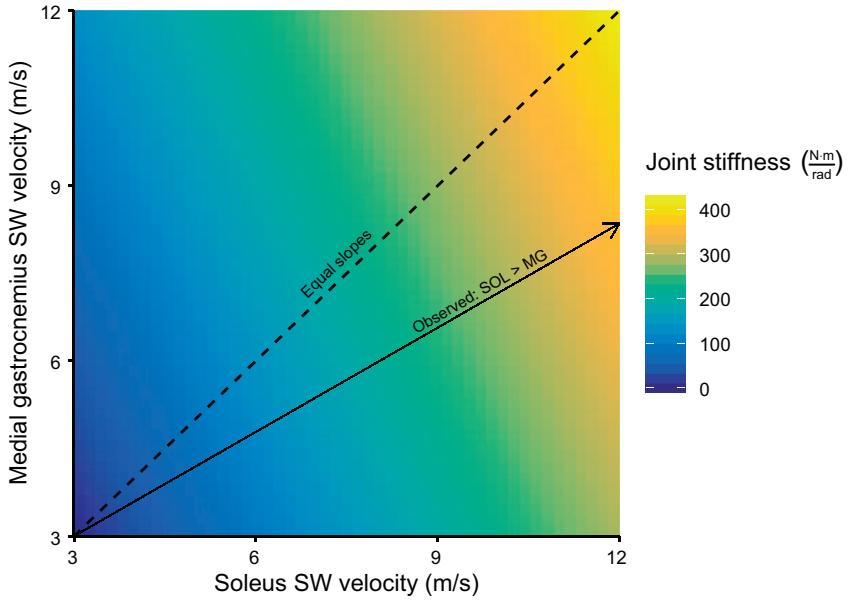

Fig. 3. Relationship between plantar flexor shear wave velocities and joint stiffness. Together, soleus and medial gastrocnemius shear wave velocities explain 96% of the variance in joint stiffness between experimental conditions. The dashed line indicates where a gradient vector of this relationship would lie if soleus and medial gastrocnemius shear wave velocities were associated with equal increases in joint stiffness (i.e., had identical slopes or parameter estimates). The solid vector represents the gradient of the observed relationship, which favors soleus shear wave velocity; this indicates that a given increase in soleus shear wave velocity is associated with a greater increase in joint stiffness than the same increase in medial gastrocnemius shear wave velocity. SW, shear wave.

Table 1. *Hierarchical linear model of joint stiffness regressed on soleus and medial gastrocnemius shear wave velocities*

Parameter	Estimate ± SE	*t*-Value
Intercept	−94.5 ± 12.2	−7.73
Soleus	29.58 ± 4.22	7.01
Medial gastrocnemius	13.20 ± 2.32	5.69

system identification analyses to evaluate joint stiffness during active conditions, independent of higher-order contributors to joint mechanical impedance (e.g., inertia and damping). We observed strong, linear relationships between ankle joint stiffness and SW velocity of the MG and SOL (Fig. 3). Herein, we describe the biomechanical basis of this relationship.

We experimentally altered plantar flexor activation to influence both joint stiffness and SW velocity, and our knee flexion condition decoupled the SOL and MG (14, 36). Recent work suggests activation-dependent SW velocity changes in a single muscle—as seen with joint stiffness changes (36)—are related to short-range stiffness, independent of force (11). In this experimental context, the presence of multiple muscles that span a joint complicates matters. We experimentally addressed the muscle redundancy problem by incorporating both a knee flexed and extended condition, which decoupled the MG and SOL (Fig. 2, *A* and *B*). Specifically, knee flexion shortened the MG but not SOL, such that the MG was placed under active insufficiency, as evidenced by the large position-by-moment interaction for MG in Fig. 2*A* and the small domain of MG SW velocities in Fig. 5*A*. This decoupling decreased collinearity between MG and SOL SW velocities ($r = 0.93$ to 0.46), allowing for increased precision of our parameter estimates for each muscle (Table 1). By experimentally changing activation and joint positions, we exploited the properties of each muscle to elucidate their respective roles in modulating joint stiffness. The changes in SW velocity and joint stiffness that were observed are directly proportional to the activation-induced changes in short-range stiffness.

Our parameter estimates for MG and SOL SW velocities in the joint stiffness-SW velocity model are remarkably consistent with literature and theoretical estimates. A muscle's stiffness is proportional to its physiological cross-sectional area divided by its optimal fiber length (19). Thus, the SOL is ~2.85-times stiffer than the MG at a given activation (60). Moreover, SW velocity-squared is theoretically proportional to stiffness (42); as such, we reconstructed our linear model using SW velocity-*squared*. In line with theory, we observed a SOL:MG slope ratio of 2.83 (Supplemental Table S3), almost exactly as expected (cf. 2.85). These results reinforce the biomechanical basis of our findings—not only are our trends consistent with theory, but so too are the parameter estimates from our statistical models.

Shear wave elastography is commonly used as a proxy for active muscle stiffness (55); however, from a theoretical perspective, the use of SW velocity as a proxy for stiffness may be confounded by the presence of tensile stress in the muscle. Timoshenko beam theory suggests that SW speeds are related to both shear modulus and longitudinal stress (42). Indeed, the stiffness of muscle is related to its force production (19), both of which share substantial variance with SW velocity (Figs. 2 and 5). Notwithstanding beam theory and stiffness-force collinearity, controlled experimental evidence suggests SW velocities are associated with changes in short-range stiffness, independent of force (10, 11). Although our results support the notion that changes in SW velocity induced by activation are related to changes in joint stiffness, further investigations relating SW velocity, force, and stiffness are required in passive and active muscle.

The experimental portion of this work demonstrates that SW ultrasound elastography can inform our understanding of activation-dependent changes in joint stiffness with muscle-level specificity. The extent of individual muscle dependency is of both scientific and clinical interest. Scientifically, these results suggest that SW ultrasound elastography may provide direct insight into the muscle redundancy problem as it applies to the joint stiffness domain, and can, therefore, be used to answer basic motor control and biomechanics questions. Clinically, SW can provide clinicians with muscle-specific insight into the etiology of changes in joint stiffness. Such knowledge may directly inform treatment; for example, selection of muscle(s) to treat with botulinum toxin. In the case of musculoskeletal pathology (e.g., hemiparesis), clinical prediction models should be developed to predict individual muscle contributions to and treatment effects on joint stiffness.

Musculoskeletal Modeling

Musculoskeletal modeling can reveal the neuromechanical underpinnings of muscle stiffness, joint stiffness, and end-point stiffness (1, 32). We used two modeling approaches to unravel the underlying MTU properties associated with greater ankle joint stiffness. The first approach employed a lumped muscle model with experimentally derived Achilles tendon stiffness, joint stiffness, net joint moment, and literature-based Achilles tendon moment arm as inputs. This model yielded physiologically implausible estimates of muscle stiffness, ranging from 13 to 78,604 N/mm, likely stemming from the method used to estimate Achilles tendon stiffness. Specifically, in tracking the MG MTJ, it was assumed that all force is transmitted through the MG subtendon, and the resulting stiffness estimate is representative of the entire tendon; however, it is important to

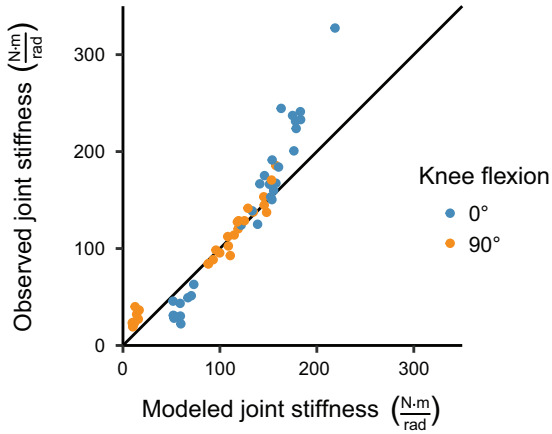

Fig. 4. Agreement between observed and modeled joint stiffness. Modeled joint stiffness agreed well with observed joint stiffness for both flexed (orange) and extended (blue) knee conditions, despite some bias in the knee-extended condition. Diagonal line indicates perfect agreement.

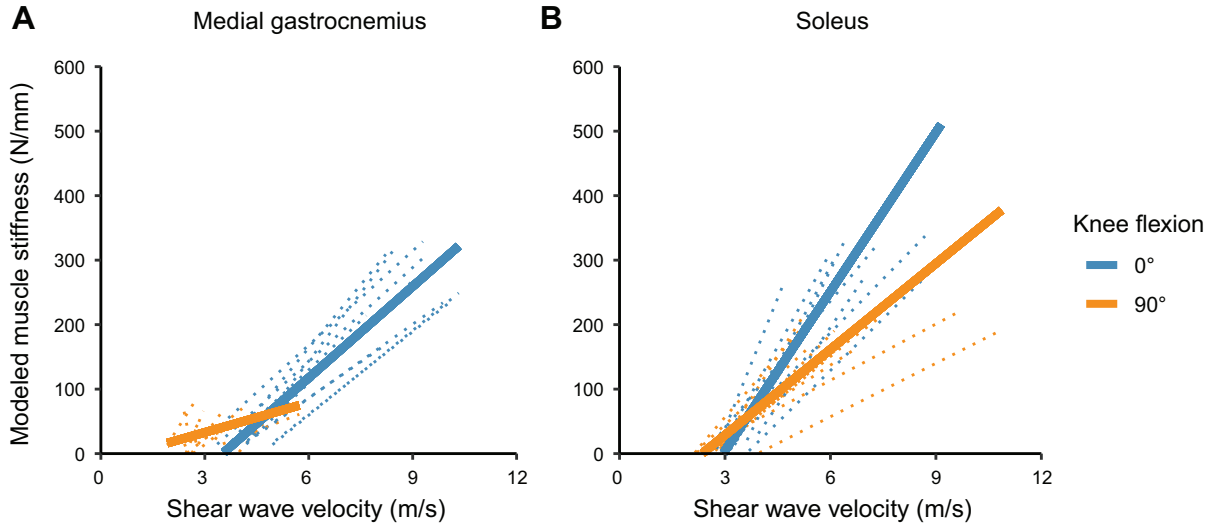

Fig. 5. Discrete muscle model stiffness outputs. *A*: relationship between medial gastrocnemius shear wave velocity and modeled medial gastrocnemius stiffness was fairly weak when the knee was flexed (orange), but strengthened when the knee was extended (blue). *B*: soleus shear wave velocity was linearly related to modeled soleus stiffness for both knee flexed and extended conditions. Solid lines indicate constant estimates (i.e., pooled or fixed effects), and dotted lines indicate varying effects (i.e., individual or random effects).

consider under what circumstances this assumption is adopted. In the case of our implementation, it is not valid. Not only is force sharing present, but differences in subtendon architecture will give rise to differences in equivalent stiffness between each of the subtendons (26). Because of the limitations of the lumped model, a second model using discrete MTUs was developed to thoroughly explore the muscle-tendon mechanics underlying the observed stiffness changes.

The discrete muscle model accurately reproduced ankle joint stiffness estimates based on task demands (Fig. 4) and supported the plausibility of the simulated MTU mechanics. After verifying the model on the joint level, modeled SOL and MG stiffness estimates were regressed on SOL and MG SW velocities. In both muscles, SW velocity explained a large proportion of the variance in modeled muscle stiffness (80–95%; Fig. 5). These results build upon previous work that verified a discrete muscle model with a single measure (end-point stiffness) rather than multiple measures (joint stiffness and SW velocity) (32). By verifying our model with multiple empirical assessments, we are more confident in both its output and the underlying processes that were modeled. The linear relationship between net joint moment and stiffness (36) can be explained by activation-dependent muscle stiffness (Fig. 4), which correlates with the SW velocity of each muscle (Fig. 5). Our discrete muscle model complements our experimental results by explaining the observed variance in our experimental results from first principles; converging evidence from different sources reinforces the biomechanical basis and validity of our findings.

Conclusion

Using SW elastography to assess the mechanical properties of muscle during isometric tasks, we found that changes in SW velocity in the plantar flexors are associated with changes in ankle joint stiffness assessed with system identification. A discrete muscle model was constructed to explore the mechanical basis of this relationship and accurately estimated joint stiffness values. The modeled muscle stiffness, which controlled modeled joint stiffness, was largely explained by changes in SW velocity. Shear wave ultrasound elastography may, therefore, be used in conjunction with joint stiffness assessments to advance our understanding of muscle-dependent changes in joint stiffness.

APPENDIX: POST HOC DISCRETE MUSCLE MODEL FORMULATION

The discrete muscle model was parameterized in accordance with previous literature (Supplemental Table S1) and was built similarly to a verified upper extremity end-point stiffness model (32). The modeling process started with calculating muscle activation, u, of each of the triceps surae muscles to meet task demands (net joint moment, M_{net}),

$$u = \min \sum_{i=1}^{3} \left(\frac{F_i^M}{F_{[i]o}^M} \right)^2 \ni M_{net} = J^T \vec{F}^M, \quad 0 \le F_i^M \le F_{[i]o}^M,$$

where F_i^M is the force of muscle (not fiber) i, $F_{[i]o}^M$ is its maximum force for its given length and velocity, and J is the 3×1 Jacobian. Each muscle's activation, u, was used to obtain muscle force $F^M = uF_o^M$. Whole muscle short-range stiffness was assumed to be proportional to muscle force,

$$k^M = \frac{\gamma F^M}{L_o^M},$$

where L_o^M is the muscle's optimal fiber length and $\gamma = 23.4$ is a unitless scaling parameter derived from animal data (19). Each muscle acts in series with its respective tendon, a Hookean spring with stiffness

$$k^T = \frac{E^T A^T}{L_s^T},$$

where E^T is elastic modulus of the tendon (28), A^T is the subtendon cross-sectional area (46), and L_s^T is subtendon slack length, which was obtained by modeling each respective MTU to have a slack length in

accordance with positions obtained empirically (31). The equivalent stiffness of the entire MTU can, thus, be modeled as

$$k_i^{MT} = \frac{k^T k^M}{k^T + k^M}.$$

Finally, because each MTU acts about a joint from a distance, the Jacobian J and its angle derivative were used to transform forces and linear stiffnesses to rotational ones; that is, ankle joint stiffness:

$$k^J = J^T \vec{K}^{MT} J + \frac{dJ}{d\theta} \vec{F}^{MT}.$$

Musculoskeletal model parameters were obtained from the literature for shank length (47), moment arms (5), muscle volume (27), optimal fiber length (5, 60), pennation angle (60), MTU length (30), MTU slack length (30, 31), tendon slack length (62), subtendon geometry (46), and tendon elasticity (28). The specific individual values and scaling equations used can be found in Supplemental Table S1, and the MATLAB code for the model can be found on the Open Science Framework: https://osf.io/5k8bw/.

ACKNOWLEDGMENTS

The authors would like to thank Dr. Daniel Ludvig for his technical assistance.

GRANTS

Research supported by the American Society of Biomechanics' Graduate Student Grant-In-Aid. This material is based upon work supported by the National Science Foundation Graduate Research Fellowship under Grant DGE-1324585.

DISCLOSURES

No conflicts of interest, financial or otherwise, are declared by the authors.

AUTHOR CONTRIBUTIONS

A.D.V., E.J.R., and S.S.L. conceived and designed research; A.D.V. performed experiments; A.D.V. analyzed data; A.D.V., E.J.R., and S.S.L. interpreted results of experiments; A.D.V. prepared figures; A.D.V. drafted manuscript; A.D.V., E.J.R., and S.S.L. edited and revised manuscript; A.D.V., E.J.R., and S.S.L. approved final version of manuscript.

ENDNOTE

At the request of the authors, readers are herein alerted to the fact that source data related to this manuscript may be found on the Open Source Framework at https://osf.io/d49pb. These source data are not a part of this manuscript, and have not undergone peer review by the American Physiological Society (APS). APS and the journal editors take no responsibility for these materials, for the website address, or for any links to or from it.

REFERENCES

1. **Agarwal GC, Gottlieb CL.** Compliance of the human ankle joint. *J Biomech Eng* 99: 166–170, 1977. doi:10.1115/1.3426285.
2. **Akagi R, Shikiba T, Tanaka J, Takahashi H.** A six-week resistance training program does not change shear modulus of the triceps brachii. *J Appl Biomech* 32: 373–378, 2016. doi:10.1123/jab.2015-0290.
3. **Akagi R, Takahashi H.** Effect of a 5-week static stretching program on hardness of the gastrocnemius muscle. *Scand J Med Sci Sports* 24: 950–957, 2014. doi:10.1111/sms.12111.
4. **Alhusaini AA, Crosbie J, Shepherd RB, Dean CM, Scheinberg A.** Mechanical properties of the plantarflexor musculotendinous unit during passive dorsiflexion in children with cerebral palsy compared with typically developing children. *Dev Med Child Neurol* 52: e101–e106, 2010. doi:10.1111/j.1469-8749.2009.03600.x.
5. **Arnold EM, Ward SR, Lieber RL, Delp SL.** A model of the lower limb for analysis of human movement. *Ann Biomed Eng* 38: 269–279, 2010. doi:10.1007/s10439-009-9852-5.
6. **Azocar AF, Rouse EJ.** Stiffness perception during active ankle and knee movement. *IEEE Trans Biomed Eng* 64: 2949–2956, 2017. doi:10.1109/TBME.2017.2691308.
7. **Bakdash JZ, Marusich LR.** Repeated measures correlation. *Front Psychol* 8: 456, 2017. doi:10.3389/fpsyg.2017.00456.
8. **Bates D, Mächler M, Bolker B, Walker S. Fitting linear mixed-effects models using lme4.** ***arXiv preprint arXiv:1406.5823*****, 2014. doi:10.18637/jss.v067.i01.**
9. **Bercoff J, Tanter M, Fink M.** Supersonic shear imaging: a new technique for soft tissue elasticity mapping. *IEEE Trans Ultrason Ferroelectr Freq Control* 51: 396–409, 2004. doi:10.1109/TUFFC.2004.1295425.
10. **Bernabei M, Lee SS, Perreault EJ, Sandercock TG.** Muscle stress provides a lower bound on the magnitude of shear wave velocity. International Society of Biomechanics/American Society of Biomechanics. 2019, Calgary, Canada, p. 1021.
11. **Bernabei M, Lee SSM, Perreault EJ, Sandercock TG.** Shear wave velocity is sensitive to changes in muscle stiffness that occur independently from changes in force. *J Appl Physiol* 128: 8–16, 2020. doi:10.1152/japplphysiol.00112.2019.
12. **Bland JM, Altman DG.** Calculating correlation coefficients with repeated observations: Part 1–Correlation within subjects. *BMJ* 310: 446, 1995. doi:10.1136/bmj.310.6977.446.
13. **Buchanan TS, Lloyd DG, Manal K, Besier TF.** Neuromusculoskeletal modeling: estimation of muscle forces and joint moments and movements from measurements of neural command. *J Appl Biomech* 20: 367–395, 2004. doi:10.1123/jab.20.4.367.
14. **Chernak LA, DeWall RJ, Lee KS, Thelen DG.** Length and activation dependent variations in muscle shear wave speed. *Physiol Meas* 34: 713–721, 2013. doi:10.1088/0967-3334/34/6/713.
15. **Chino K, Takahashi H.** The association of muscle and tendon elasticity with passive joint stiffness: In vivo measurements using ultrasound shear wave elastography. *Clin Biomech (Bristol, Avon)* 30: 1230–1235, 2015. doi:10.1016/j.clinbiomech.2015.07.014.
16. **Chino K, Takahashi H.** Measurement of gastrocnemius muscle elasticity by shear wave elastography: association with passive ankle joint stiffness and sex differences. *Eur J Appl Physiol* 116: 823–830, 2016. doi:10.1007/s00421-016-3339-5.
17. **Chino K, Takashi H.** Association of gastrocnemius muscle stiffness with passive ankle joint stiffness and sex-related difference in the joint stiffness. *J Appl Biomech* 34: 169–174, 2018. doi:10.1123/jab.2017-0121.
18. **Crowninshield RD, Brand RA.** The prediction of forces in joint structures; distribution of intersegmental resultants. *Exerc Sport Sci Rev* 9: 159–182, 1981. doi:10.1249/00003677-198101000-00004.
19. **Cui L, Perreault EJ, Maas H, Sandercock TG.** Modeling short-range stiffness of feline lower hindlimb muscles. *J Biomech* 41: 1945–1952, 2008. doi:10.1016/j.jbiomech.2008.03.024.
20. **Cumming G.** The new statistics: why and how. *Psychol Sci* 25: 7–29, 2014. doi:10.1177/0956797613504966.
21. **Delp SL, Anderson FC, Arnold AS, Loan P, Habib A, John CT, Guendelman E, Thelen DG.** OpenSim: open-source software to create and analyze dynamic simulations of movement. *IEEE Trans Biomed Eng* 54: 1940–1950, 2007. doi:10.1109/TBME.2007.901024.
22. **Farcy S, Nordez A, Dorel S, Hauraix H, Portero P, Rabita G.** Interaction between gastrocnemius medialis fascicle and Achilles tendon compliance: a new insight on the quick-release method. *J Appl Physiol (1985)* 116: 259–266, 2014. doi:10.1152/japplphysiol.00309.2013.
23. **Franz JR, Khanchandani A, McKenny H, Clark WH.** Ankle rotation and muscle loading effects on the calcaneal tendon moment arm: an in vivo imaging and modeling study. *Ann Biomed Eng* 47: 590–600, 2019. doi:10.1007/s10439-018-02162-4.
24. **Gardner MJ, Altman DG.** Confidence intervals rather than *P* values: estimation rather than hypothesis testing. *Br Med J (Clin Res Ed)* 292: 746–750, 1986. doi:10.1136/bmj.292.6522.746.
25. **Gennisson JL, Deffieux T, Macé E, Montaldo G, Fink M, Tanter M.** Viscoelastic and anisotropic mechanical properties of in vivo muscle tissue assessed by supersonic shear imaging. *Ultrasound Med Biol* 36: 789–801, 2010. doi:10.1016/j.ultrasmedbio.2010.02.013.
26. **Handsfield GG, Inouye JM, Slane LC, Thelen DG, Miller GW, Blemker SS.** A 3D model of the Achilles tendon to determine the mechanisms underlying nonuniform tendon displacements. *J Biomech* 51: 17–25, 2017. doi:10.1016/j.jbiomech.2016.11.062.
27. **Handsfield GG, Meyer CH, Hart JM, Abel MF, Blemker SS.** Relationships of 35 lower limb muscles to height and body mass quantified

using MRI. *J Biomech* 47: 631–638, 2014. doi:10.1016/j.jbiomech.2013.12.002.
28. **Hansen P, Kovanen V, Hölmich P, Krogsgaard M, Hansson P, Dahl M, Hald M, Aagaard P, Kjaer M, Magnusson SP.** Micromechanical properties and collagen composition of ruptured human achilles tendon. *Am J Sports Med* 41: 437–443, 2013. doi:10.1177/0363546512470617.
29. **Hashizume S, Iwanuma S, Akagi R, Kanehisa H, Kawakami Y, Yanai T.** The contraction-induced increase in Achilles tendon moment arm: a three-dimensional study. *J Biomech* 47: 3226–3231, 2014. doi:10.1016/j.jbiomech.2014.08.003.
30. **Hawkins D, Hull ML.** A method for determining lower extremity muscle-tendon lengths during flexion/extension movements. *J Biomech* 23: 487–494, 1990. doi:10.1016/0021-9290(90)90304-L.
31. **Hirata K, Kanehisa H, Miyamoto-Mikami E, Miyamoto N.** Evidence for intermuscle difference in slack angle in human triceps surae. *J Biomech* 48: 1210–1213, 2015. doi:10.1016/j.jbiomech.2015.01.039.
32. **Hu X, Murray WM, Perreault EJ.** Muscle short-range stiffness can be used to estimate the endpoint stiffness of the human arm. *J Neurophysiol* 105: 1633–1641, 2011. doi:10.1152/jn.00537.2010.
33. **Hug F, Tucker K, Gennisson JL, Tanter M, Nordez A.** Elastography for muscle biomechanics: toward the estimation of individual muscle force. *Exerc Sport Sci Rev* 43: 125–133, 2015. doi:10.1249/JES.0000000000000049.
34. **Ichihashi N, Umegaki H, Ikezoe T, Nakamura M, Nishishita S, Fujita K, Umehara J, Nakao S, Ibuki S.** The effects of a 4-week static stretching programme on the individual muscles comprising the hamstrings. *J Sports Sci* 34: 2155–2159, 2016. doi:10.1080/02640414.2016.1172725.
35. **Jakubowski KL, Terman A, Santana RVC, Lee SSM.** Passive material properties of stroke-impaired plantarflexor and dorsiflexor muscles. *Clin Biomech (Bristol, Avon)* 49: 48–55, 2017. doi:10.1016/j.clinbiomech.2017.08.009.
36. **Kearney RE, Hunter IW.** System identification of human joint dynamics. *Crit Rev Biomed Eng* 18: 55–87, 1990.
37. **Latash ML, Zatsiorsky VM.** Joint stiffness: myth or reality? *Hum Mov Sci* 12: 653–692, 1993. doi:10.1016/0167-9457(93)90010-M.
38. **Lee SS, Gaebler-Spira D, Zhang LQ, Rymer WZ, Steele KM.** Use of shear wave ultrasound elastography to quantify muscle properties in cerebral palsy. *Clin Biomech (Bristol, Avon)* 31: 20–28, 2016. doi:10.1016/j.clinbiomech.2015.10.006.
39. **Lee SS, Spear S, Rymer WZ.** Quantifying changes in material properties of stroke-impaired muscle. *Clin Biomech (Bristol, Avon)* 30: 269–275, 2015. doi:10.1016/j.clinbiomech.2015.01.004.
40. **Lin LI.** A concordance correlation coefficient to evaluate reproducibility. *Biometrics* 45: 255–268, 1989. doi:10.2307/2532051.
41. **Ludvig D, Perreault EJ.** System identification of physiological systems using short data segments. *IEEE Trans Biomed Eng* 59: 3541–3549, 2012. doi:10.1109/TBME.2012.2220767.
42. **Martin JA, Brandon SCE, Keuler EM, Hermus JR, Ehlers AC, Segalman DJ, Allen MS, Thelen DG.** Gauging force by tapping tendons. *Nat Commun* 9: 1592, 2018. doi:10.1038/s41467-018-03797-6.
43. **McShane BB, Gal D, Gelman A, Robert C, Tackett JL.** Abandon statistical significance. *Am Stat* 73, *Supp1*: 235–245, 2019. doi:10.1080/00031305.2018.1527253.
44. **Nakagawa S, Johnson PCD, Schielzeth H.** The coefficient of determination R^2 and intra-class correlation coefficient from generalized linear mixed-effects models revisited and expanded. *J R Soc Interface* 14: 20170213, 2017. doi:10.1098/rsif.2017.0213.
45. **Pedotti A, Krishnan VV, Stark L.** Optimization of muscle-force sequencing in human locomotion. *Math Biosci* 38: 57–76, 1978. doi:10.1016/0025-5564(78)90018-4.
46. **Pękala PA, Henry BM, Ochała A, Kopacz P, Tatoń G, Młyniec A, Walocha JA, Tomaszewski KA.** The twisted structure of the Achilles tendon unraveled: A detailed quantitative and qualitative anatomical investigation. *Scand J Med Sci Sports* 27: 1705–1715, 2017. [Erratum in *Scand J Med Sci Sports* 27: 1705–1715, 2017.] doi:10.1111/sms.12835.
47. **Plagenhoef S, Evans FG, Abdelnour T.** Anatomical data for analyzing human motion. *Res Q Exerc Sport* 54: 169–178, 1983. doi:10.1080/02701367.1983.10605290.
48. **R Core Development Team.** *R: A language and environment for statistical computing*. Vienna, Austria: R Foundation for Statistical Computing, 2017.
49. **Raiteri BJ, Cresswell AG, Lichtwark GA.** Ultrasound reveals negligible cocontraction during isometric plantar flexion and dorsiflexion despite the presence of antagonist electromyographic activity. *J Appl Physiol (1985)* 118: 1193–1199, 2015. doi:10.1152/japplphysiol.00825.2014.
50. **Rao SR, Saltzman CL, Wilken J, Yak HJ.** Increased passive ankle stiffness and reduced dorsiflexion range of motion in individuals with diabetes mellitus. *Foot Ankle Int* 27: 617–622, 2006. doi:10.1177/107110070602700809.
51. **Rouse EJ, Gregg RD, Hargrove LJ, Sensinger JW.** The difference between stiffness and quasi-stiffness in the context of biomechanical modeling. *IEEE Trans Biomed Eng* 60: 562–568, 2013. doi:10.1109/TBME.2012.2230261.
52. **Rouse EJ, Hargrove LJ, Perreault EJ, Kuiken TA.** Estimation of human ankle impedance during the stance phase of walking. *IEEE Trans Neural Syst Rehabil Eng* 22: 870–878, 2014. doi:10.1109/TNSRE.2014.2307256.
53. **Sepehri B, Esteki A, Ebrahimi-Takamjani E, Shahidi GA, Khamseh F, Moinodin M.** Quantification of rigidity in Parkinson's disease. *Ann Biomed Eng* 35: 2196–2203, 2007. doi:10.1007/s10439-007-9379-6.
54. **Shorter AL, Rouse EJ.** Mechanical impedance of the ankle during the terminal stance phase of walking. *IEEE Trans Neural Syst Rehabil Eng* 26: 135–143, 2018. doi:10.1109/TNSRE.2017.2758325.
55. **Taljanovic MS, Gimber LH, Becker GW, Latt LD, Klauser AS, Melville DM, Gao L, Witte RS.** Shear-wave elastography: basic physics and musculoskeletal applications. *Radiographics* 37: 855–870, 2017. doi:10.1148/rg.2017160116.
56. **Thilmann AF, Fellows SJ, Ross HF.** Biomechanical changes at the ankle joint after stroke. *J Neurol Neurosurg Psychiatry* 54: 134–139, 1991. doi:10.1136/jnnp.54.2.134.
57. **Vigotsky AD, Rouse EJ, Lee SSM.** In vivo relationship between joint stiffness, joint-based estimates of muscle stiffness, and shear-wave velocity. American Society of Biomechanics 42nd Annual Meeting. Rochester, MN, 2018.
58. **Vigotsky AD, Rouse EJ, Lee SSM.** In vivo relationship between joint stiffness, joint-based estimates of muscle stiffness, and shear-wave velocity. *Conf Proc IEEE Eng Med Biol Soc* 2018: 1468–1471, 2018. doi:10.1109/EMBC.2018.8512484.
59. **Vigotsky AD, Schoenfeld BJ, Than C, Brown JM.** Methods matter: the relationship between strength and hypertrophy depends on methods of measurement and analysis. *PeerJ* 6: e5071, 2018. doi:10.7717/peerj.5071.
60. **Ward SR, Eng CM, Smallwood LH, Lieber RL.** Are current measurements of lower extremity muscle architecture accurate? *Clin Orthop Relat Res* 467: 1074–1082, 2009. doi:10.1007/s11999-008-0594-8.
61. **Werkhausen A, Albracht K, Cronin NJ, Paulsen G, Bojsen-Møller J, Seynnes OR.** Effect of training-induced changes in Achilles tendon stiffness on muscle-tendon behavior during landing. *Front Physiol* 9: 794, 2018. doi:10.3389/fphys.2018.00794.
62. **Zajac FE.** Muscle and tendon: properties, models, scaling, and application to biomechanics and motor control. *Crit Rev Biomed Eng* 17: 359–411, 1989.